ECOPHYSIOLOGY, STRESS AND ADAPTATION

Physiologia Plantarum

In contrast to diatoms, cryptophytes are susceptible to iron limitation, but not to ocean acidification

Marianne G. Camoying[1] 🄾 | Silke Thoms[1] | Jana K. Geuer[1] | Boris P. Koch[1,2] | Kai Bischof[3] | Scarlett Trimborn[1,3]

[1]Ecological Chemistry, Alfred Wegener Institute, Helmholtz Centre for Polar and Marine Research, Bremerhaven, Germany

[2]Department of Technology, University of Applied Sciences Bremerhaven, Bremerhaven, Germany

[3]Marine Botany & MARUM, University of Bremen, Bremen, Germany

Correspondence
Marianne G. Camoying, Ecological Chemistry, Alfred Wegener Institute, Helmholtz Centre for Polar and Marine Research, Bremerhaven, Germany.
Email: marianne.camoying@awi.de

Abstract

Previous field studies in the Southern Ocean (SO) indicated an increased occurrence and dominance of cryptophytes over diatoms due to climate change. To gain a better mechanistic understanding of how the two ecologically important SO phytoplankton groups cope with ocean acidification (OA) and iron (Fe) availability, we chose two common representatives of Antarctic waters, the cryptophyte *Geminigera cryophila* and the diatom *Pseudo-nitzschia subcurvata*. Both species were grown at 2°C under different pCO_2 (400 vs. 900 μatm) and Fe (0.6 vs. 1.2 nM) conditions. For *P. subcurvata*, an additional high pCO_2 level was applied (1400 μatm). At ambient pCO_2 under low Fe supply, growth of *G. cryophila* almost stopped while it remained unaffected in *P. subcurvata*. Under high Fe conditions, OA was not beneficial for *P. subcurvata*, but stimulated growth and carbon production of *G. cryophila*. Under low Fe supply, *P. subcurvata* coped much better with OA than the cryptophyte, but invested more energy into photoacclimation. Our study reveals that Fe limitation was detrimental for the growth of *G. cryophila* and suppressed the positive OA effect. The diatom was efficient in coping with low Fe, but was stressed by OA while both factors together strongly impacted its growth. The distinct physiological response of both species to OA and Fe limitation explains their occurrence in the field. Based on our results, Fe availability is an important modulator of OA effects on SO phytoplankton, with different implications on the occurrence of cryptophytes and diatoms in the future.

1 | INTRODUCTION

The Southern Ocean (SO) is considered as a High-Nutrient, Low-Chlorophyll (HNLC) region, wherein primary productivity is mainly influenced by the availability of the trace metal iron (Fe; Martin et al., 1990; De Baar et al., 1995; Smetacek et al., 2012). Fe plays a major role in various cellular processes such as photosynthesis, respiration, and carbon and nitrogen fixation. Fe-limited phytoplankton cells normally exhibit lowered photochemical quantum efficiency

(Greene et al., 1991, 1992; Marchetti et al., 2006, 2017) and reduced cellular pigment concentrations (van Leeuwe et al., 2014), leading to less-efficient electron transport (Greene et al., 1991). Fe limitation also results in reduced growth and particulate organic carbon (POC) production (Alderkamp et al., 2012; Koch et al., 2018; Petrou et al., 2014; Trimborn et al., 2019a). To deal with low Fe availability, SO phytoplankton were also found to lower their Fe requirement by replacing the Fe-rich electron transporter cytochrome c6 with the Cu-containing plastocyanin (Peers & Price, 2006).

Due to ongoing CO_2 emissions into the atmosphere, SO phytoplankton will be affected by ocean acidification (OA), which is the decrease in ocean pH due to the oceanic absorption of atmospheric CO_2. Hence, the current partial pressure of CO_2 (pCO_2) in seawater of ca. 410 μatm is projected to double by the end of this century (IPCC, 2014). In response to OA, changes in community structure and/or productivity of SO natural phytoplankton assemblages were found (Davidson et al., 2016; Donahue et al., 2019; Feng et al., 2010; Hancock et al., 2018; Heiden et al., 2019; Hoppe et al., 2013; Thomson et al., 2016; Tortell et al., 2008; Trimborn et al., 2017a). Only a few studies (Coad et al., 2016; McMinn et al., 2014; Young et al., 2015) have reported no OA effect on SO phytoplankton. At present, studies looking at the combined effects of OA and Fe availability on the ecophysiology of SO phytoplankton are limited (Hoppe et al., 2013; Koch et al., 2018), which could be attributed to the difficulty in conducting experiments under trace metal clean conditions. In combination with Fe limitation, OA was shown to promote species shifts and/or hamper primary production of natural SO phytoplankton assemblages (Feng et al., 2010; Hoppe et al., 2013; Tortell et al., 2008; Trimborn et al., 2017b). It was observed that growth of the diatoms *Chaetoceros* (Feng et al., 2010; Hoppe et al., 2013; Tortell et al., 2008) and *Fragilariopsis* (Davidson et al., 2016; Heiden et al., 2019) or of the prymnesiophyte *Phaeocystis antarctica* (Trimborn et al., 2017b) was promoted by OA. The tolerance of the genus *Phaeocystis* to OA in combination with different environmental factors such as light and Fe was previously reported (Feng et al., 2010; Hancock et al., 2018; Heiden et al., 2019; Hoogstraten et al., 2012; Koch et al., 2018; Thoisen et al., 2015; Tortell et al., 2008; Trimborn et al., 2017b; Trimborn et al., 2019a; Young et al., 2015; Zhu et al., 2017). While a specific strain of the diatom *Pseudo-nitzschia subcurvata* showed no susceptibility to OA (even up to 1730 ppm pCO_2; Zhu et al., 2017), other studies reported an OA-dependent decline in the growth of several *Pseudo-nitzschia* species (another *P. subcurvata* strain, *Pseudo-nitzschia turgiduloides*, *Pseudo-nitzschia turgiduloides prolongatoides*) regardless of Fe availability (Hancock et al., 2018; Hoppe et al., 2013; Trimborn et al., 2017b). It is evident from these observations that different taxa have specific CO_2-tolerance levels. However, a mechanistic understanding of these responses is still lacking, specifically for the genus *Pseudo-nitzschia*, which contributes significantly to the total diatom blooms in the SO (Almandoz et al., 2008; Garibotti et al., 2003).

The effects of climate change in different regions of the SO are now becoming more evident. The Western Antarctic Peninsula (WAP), for example, has been experiencing rapid warming over the past decades (Henley et al., 2019; Kerr et al., 2018; Moffat & Meredith, 2018), which has led to changes in the observed occurrence and distribution of various phytoplankton groups of this region (Garibotti & Ferrario, 2005; Montes-Hugo et al., 2009). It is now widely recognized that next to diatoms, cryptophytes also significantly contribute to phytoplankton biomass in the coastal regions of the WAP (Moline & Prézelin, 1996; Moline et al., 2004; Mendes et al., 2013, 2017; Schofield et al., 2017; Brown et al., 2021). Previous studies have shown that diatoms and cryptophytes have distinct ecological niches and typically do not co-occur spatially and temporally (Garibotti et al., 2003; Schofield et al., 2017). Since the dominance of cryptophytes in the field are associated with lower temperature and salinity brought by the increase in sea ice retreat and glacial melting (Moline et al., 2004; Mendes et al., 2013; Schofield et al., 2017), cryptophytes may thus appear to be the winners of the ongoing climatic changes in the SO. However, studies looking at the effects of different environmental factors (OA, Fe, light) on the ecophysiology of this group are still limited. To date, only two studies are available on Antarctic cryptophytes, which show that OA and high light promoted growth and POC production of *Geminigera cryophila* (Trimborn et al., 2019b) while Fe limitation, on the other hand, strongly impacted its growth and photophysiology (Koch et al., 2018). Our study aims to gain a better understanding of the ecophysiology of two key Antarctic phytoplankton species, the cryptophyte *G. cryophila* and the diatom *Pseudo-nitzschia subcurvata*, in response to OA and Fe limitation.

2 | MATERIALS AND METHODS

2.1 | Culture conditions

Prior to the initiation of the experiment, the Antarctic diatom *Pseudo-nitzschia subcurvata* (isolated by P. Assmy, Polarstern expedition ANT-XXI/4) and the Southern Ocean cryptophyte *G. cryophila* (CCMP 2564), were kept for more than a year in stock cultures with Fe-deplete and -replete natural Antarctic seawater medium. Before the start of the main experiment, both species were pre-acclimated for at least 2 weeks under the target experimental conditions (CO_2 and Fe), which will be described below. The sterile-filtered (0.2 μm), Fe-poor (0.12 nmol L^{-1}) Antarctic seawater collected during the Antarctic Circumpolar Expedition (59°S) was enriched with macronutrients (100 μmol L^{-1} Si, 100 μmol L^{-1} NO_3^-, and 6.25 μmol L^{-1} PO_4^{3-}) and vitamins (30 nmol L^{-1} B_1, 23 nmol L^{-1} B_7, and 0.228 nmol L^{-1} B_{12}), which were chelated (Chelex® 100, Sigma Aldrich, Merck) to remove any trace metals present. Nitrate and phosphate were added following the Redfield N:P ratio of 16:1 (Redfield, 1958). For the pre-acclimation phase and the main experiment, dilute batch cultures of both species were grown in this seawater, to which either a trace metal (TM) mix containing no Fe (i.e. Control treatment) or 0.5 nmol L^{-1} Fe (FeCl$_3$, ICP-MS standard, TraceCERT, Fluka; i.e. +Fe treatment) was added. The TM mixture contained zinc (0.16 nmol L^{-1}), copper (0.08 nmol L^{-1}), cobalt (0.09 nmol L^{-1}), molybdenum (0.05 nmol L^{-1}), and manganese (1.9 nmol L^{-1}). These TM additions were adjusted to maintain the ratio of the original F/2 recipe and represent trace metal concentrations typical for SO waters. The total dissolved Fe concentration [dFe] of our Control treatments represents the [dFe] values measured in the upper surface mixed layer of SO waters (0.1–0.3 nM Fe, Klunder et al., 2011). On the other hand, +Fe treatments mimic [dFe] values representative for coastal regions of the SO or during natural Fe supply events (e.g. vertical mixing, upwelling) (1–2 nM Fe, Klunder et al., 2014). As suggested by Gerringa et al. (2000), in an effort to minimize the alteration of the natural seawater trace metal chemistry and ligands, no ethylenediaminetetraacetic acid (EDTA) was added. Due to the presence of natural ligands, it is expected that the added Fe was buffered rather than bound in complexed inorganic colloids. TM clean techniques were employed throughout the whole experiment. 4 L polycarbonate (PC) incubation bottles, tubings, and all

other equipment were TM cleaned according to the Geotraces cookbook (Cutter et al., 2017), as previously described in Koch et al. (2018). All sampling and handling of the incubation bottles were conducted under the laminar flow hood (US class 100, Opta). Both species were also grown under the target pCO_2 levels of 400 and 900 µatm (i.e. 400 and 900 treatment, respectively). Only *P. subcurvata* was additionally grown at 1400 µatm pCO_2 (i.e. 1400 treatment). The three different pCO_2 levels were attained by gentle bubbling of the culture bottles with humidified CO_2 air. A mixture of CO_2-free air (<1 ppmv CO_2; Dominic Hunter) and pure CO_2 (Air Liquide Deutschland Ltd.) was used and controlled through a gas flow controller (CGM 2000, MCZ Umwelttechnik) to generate the three target pCO_2 treatments. Triplicates of each experimental treatment were grown at 2°C and exposed to 100 µmol photons m^{-2} s^{-1} under a light/dark cycle of 16/8 h using light-emitting diodes (LED) lamps (SolarStinger LED SunStrip Daylight, Econlux).

2.1.1 | Carbonate chemistry determination

To ensure that there would be no pH drift (≤ 0.06 pH units) in cultures, the pH (NBS) was measured regularly in all incubation and culture medium bottles throughout the whole experiment. The pH was measured using a pH meter (826 pH mobile, Metrohm), calibrated (3-point calibration) prior to usage. The pH of all treatments was stable (Table 1). At the end of the experiment, samples for total alkalinity (TA) analysis were collected from all incubations and culture medium bottles by filtering a sample through a glass fiber filter (GF/F, Whatman) and placing the filtrate into 200-ml borosilicate flasks. TA samples were measured by potentiometric titrations via a TW alpha plus (SI Analytics). Systematic errors were corrected with a certified reference material (from A. Dickson; batch no. 161). TA, pH, silicate, phosphate, temperature, and salinity measurements were used to determine the seawater carbonate chemistry using the CO2Sys program (Pierrot et al., 2006), wherein the equilibrium constant of Mehrbach et al. (1973) refitted by Dickson and Millero (1987) was used.

2.1.2 | Concentrations of total dissolved Fe in seawater, domoic acid, and cellular trace metal quotas

To determine the concentration of total Fe dissolved [dFe] in seawater, all culture medium and incubation bottles were sampled at the end of the experiments. To this end, 100 ml of each sample was filtered (HCl-cleaned 0.2 µm PC filters, 47 mm, Nuclepore, Whatman, GE Healthcare) under a laminar flow hood and stored in TM cleaned PE bottles. Total dissolved Fe (dFe) concentrations of all seawater samples and process blanks were determined as previously described in Koch and Trimborn (2019). Results of the analysis were validated by analyzing a NASS-7 (National Research Council of Canada) reference standard in a 1:10 dilution, which was done at the beginning and end of each batch run. Measured dFe values (361 ± 16 ng L^{-1}, $n = 12$) did not vary from the certified reference (351 ± 26 ng L^{-1}).

Intracellular TM (Fe, Zn, Mn, Zn, and Co) quotas were determined by collecting phytoplankton cells onto 0.2 µm acid-cleaned PC filters (EMD Millipore). To remove the trace metals attached to the cell surface, the filters were rinsed (15 min) with 0.1 M oxalic acid wash (Hassler & Schoemann, 2009), followed by a filtered seawater rinse before finally storing them into TM-cleaned 30-ml polytetrafluoroethylene vials. Intracellular TM contents were analyzed via ICP-MS (Attom, Nu Instruments) following digestion with HNO_3 and HF, as previously described in Koch and Trimborn (2019). To ensure low background TM values and good digestion quality, acid (5 ml of subboiled HNO_3, 0.5 ml HF) and two filter blanks, as well as the BCR-414 (Plankton reference material, Sigma Aldrich) samples, were also processed and analyzed via ICP-MS (Table S1).

We also examined whether our *P. subcurvata* strain can produce domoic acid (DA) since it has been reported that under low Fe supply, many temperate *Pseudo-nitzschia* species produce DA, which can act as an Fe-binding ligand (Maldonado et al., 2002; Rue & Bruland, 2001). Moreover, it has also been shown that DA production in *Pseudo-nitzschia multiseries* can be influenced by pH (Lundholm et al., 2004; Trimborn et al., 2008). Hence, we collected samples for DA (dissolved and particulate forms) measurements as described in Geuer et al. (2020). In contrast to the study by Olesen et al. (2021), which reported the presence of DA in several *P. subcurvata* strains, no DA was extracted from the cells and the culture medium of all our treatments, indicating that our *P. subcurvata* strain was unable to produce DA (data not shown).

2.1.3 | Cell density and volume

During the pre-acclimation period, as well as during the main experiments, we regularly monitored the cell density of both species to ensure that exponential growth was reached and maintained for all treatments. To avoid any changes in carbonate chemistry, we diluted our culture bottles before cell densities reached ca. 15,000 cells/ml for *G. cryophila* and

TABLE 1 The CO2Sys program (Pierrot et al., 2006) was used to calculate the dissolved inorganic carbon (DIC) concentrations and partial pressure of CO_2 (pCO_2) from the measured total alkalinity (TA), pH, silicate, phosphate, salinity, and temperature. For all parameters, values are given for all culture bottles of each pCO_2 treatment at the end of the experiment, representing the means and SD ($n = 6$). Significant differences between treatments (post hoc tests) are indicated by varying lower case letters in superscript ($P < 0.05$)

Target pCO_2 (µatm)	Calculated pCO_2 (µatm)	Calculated DIC (µmol kg^{-1})	Measured pH (NBS)	Measured TA (µmol kg^{-1})
400	405 ± 56[a]	2342 ± 35[a]	8.14 ± 0.06[a]	2492 ± 41[a]
900	868 ± 33[b]	2426 ± 17[b]	7.82 ± 0.02[b]	2467 ± 22[a]
1400	1387 ± 64[c]	2507 ± 18[c]	7.65 ± 0.02[c]	2488 ± 13[a]

150,000 cells ml^{-1} for *P. subcurvata*. The main experiments were started only when the cultures maintained exponential growth. The initial cell density of the main experiment was ca. 500 cells ml^{-1} for *G. cryophila* and 5,000 cells ml^{-1} for *P. subcurvata*. The main experiment lasted between 5 and 7 days for *P. subcurvata* and between 10 and 15 days for *G. cryophila*, depending on the treatment. The final cell density of the main experiment was ca. 3000–9000 cells ml^{-1} for *G. cryophila* and 100,000–140,000 cells ml^{-1} for *P. subcurvata*. Samples for cell density and size determination were collected at the same time of the day at the start, during, and at the end of the main experiment. For *P. subcurvata*, samples were fixed with 10% acidic Lugol's solution and stored in the dark at 2°C. Utermöhl chambers (Hydrobios) were prepared and allowed to settle for 24 h before counting at least 400 cells under an inverted microscope (Axio Observer D1; Zeiss). For *G. cryophila*, a Beckman Multisizer^{TM} 3 Coulter Counter® was used to determine cell density immediately after sampling. For both species, growth rates (d^{-1}), denoted by the growth rate coefficient (μ), were calculated using the formula:

$$\mu = \ln(N_t : N_0)/t$$

where N_t refers to the cell density during the final harvest and N_0 to the one at the start of the experiment. The duration between both sampling points is represented by t. According to Hillebrand et al. (1999), cell volume was estimated for each species.

2.1.4 | Elemental carbon and nitrogen composition

Samples for POC and nitrogen (PON) were collected by gently filtering (<20 mm Hg) cultures onto precombusted glass fiber filters (15 h, 200°C, GF/F, ~0.6 μm, 25 mm, Whatman). Filters were acidified with 200 μl of 0.2 M HCl and oven-dried (> 12 h, 60°C) before analyzing them on an automated carbon nitrogen elemental analyzer (EURO EA-CN Elemental Analyzer, HEKAtech GmbH). The blank-corrected quotas were normalized with the filtered volume and cell volume. To calculate daily production rates, cellular quotas were multiplied by the corresponding growth rate of the respective treatment.

2.1.5 | Pigments

Pigment samples were collected by filtering the cultures onto GF/F filters (~0.6 μm, 25 mm, Whatman) and directly frozen in liquid nitrogen. As previously described in Trimborn et al. (2019b), the concentrations of chlorophyll *a* (Chl *a*) and c$_2$ (Chl c$_2$), fucoxanthin (Fuco), diatoxanthin (Dt), diadinoxanthin (Dd), and alloxanthin (Allo) were measured on a reversed phase high-performance liquid chromatography on a LaChromEliteR system equipped with a chilled autosampler L-2200 and a DAD detector L-2450 (VWR-Hitachi International GmbH). Peak detection, identification, and quantification were made with pigment standards (DHI Lab Products) using the EZChrom Elite software version 3.1.3. (Agilent Technologies).

2.1.6 | Photophysiological parameters

A Fast Repetition Rate fluorometer (FastOcean PTX) coupled with a FastAct Laboratory system (both from Chelsea Technologies Group Ltd.) was used to assess the photophysiological response of *P. subcurvata* and *G. cryophila* under all pCO$_2$-Fe treatments at the end of the experiment. After dark-adaption for 10 min at 2°C, the minimum Chl *a* fluorescence (F_0) was recorded. To gradually saturate photosystems II (PSII), a single turn-over flashlet of 1.2×10^{22} photons m^{-2} s^{-1} and a wavelength of 450 nm was applied, consisting of 100 flashlets on a 2 μs pitch. Subsequently, a relaxation phase of 40 flashlets on a 50 μs pitch was applied. This combination of saturation-relaxation phases was reiterated six times for every acquisition. To determine the maximum (F_m) Chl *a* fluorescence, the saturation phase of the single turnover was fitted according to Kolber et al. (1998). The dark-adapted maximum quantum yield of photosynthesis of PSII (F_v/F_m) was then calculated using the equation:

$$F_v/F_m = (F_m - F_0)/F_m$$

Fluorescence light curves (FLC) were also recorded, exposing cells to increasing light intensities for 5 min. After each light intensity, six Chl *a* fluorescence measurements were carried out. The light–adapted minimum (F') and maximum (F_m') Chl *a* fluorescence of the single turn-over acquisition was estimated from these measurements. The effective PSII quantum yield under ambient light (F_q'/F_m') was calculated according to the equation (($F_m' - F'$)/F_m') (Genty et al., 1989). The electron transport rates (ETR) were calculated following Suggett et al. (2004, 2009):

$$ETR = \sigma_{PSII} \times \left[(F_q'/F_m')/(F_v/F_m) \right] \times E$$

where E is the instantaneous irradiance (photons m^{-2} s^{-1}). Irradiance-dependent ETRs were curve-fitted according to Ralph and Gademann (2005) to determine maximum ETR (ETR$_{max}$), minimum saturating irradiance (I_k) and maximum light utilization efficiency (α). Non-photochemical quenching (NPQ) was calculated using the Stern–Volmer equation:

$$NPQ = F_m/F_m' - 1.$$

2.1.7 | Statistical analysis

A two-way analysis of variance (ANOVA) (SigmaPlot 12.3, SysStat Software Inc.) was used to evaluate the combined effects of pCO$_2$ and Fe availability on each physiological parameter. Standard *t*-tests were performed to determine direct effects between two specific treatments. Test for normality (Shapiro–Wilk) and post hoc tests (Holm–Sidak method) were also conducted (α = 0.05), and in cases wherein datasets were not normally distributed, Mann–Whitney rank sum test was used.

2.2 | Results

2.2.1 | Seawater chemistry

At the end of the experiment, TA remained the same, while DIC increased and pH decreased with increasing pCO_2 ($P = 0.002$, Table 1). In the +Fe culture medium bottles (without cells), [dFe] of the 400 was higher compared to the 900 ($P = 0.001$) and 1400 ($P < 0.001$) treatments, with the latter two pCO_2 treatments exhibiting no difference in dFe values (Figure 1A). The concentrations of dFe in the Control culture medium bottles were not affected by increasing pCO_2. For all pCO_2 levels, the Control culture medium bottles had significantly lower dFe concentration than the Fe-enriched treatments ($P < 0.001$). For all incubation bottles of both species, increasing pCO_2 had no effect on dFe concentrations (Figure 1B,C). In P. subcurvata, significantly higher dFe values were seen in the +Fe compared to the Control treatments under all pCO_2 levels ($P < 0.001$). For G. cryophila, no differences in dFe concentrations were observed between the Control and +Fe at 400, while at 900 the +Fe had 81% higher dFe than the Control ($P = 0.02$).

2.2.2 | Photosynthetic yield

For P. subcurvata (Figure 2A), the increase in pCO_2 did not influence F_v/F_m of +Fe cells, whereas, in the Control, F_v/F_m remained unaltered
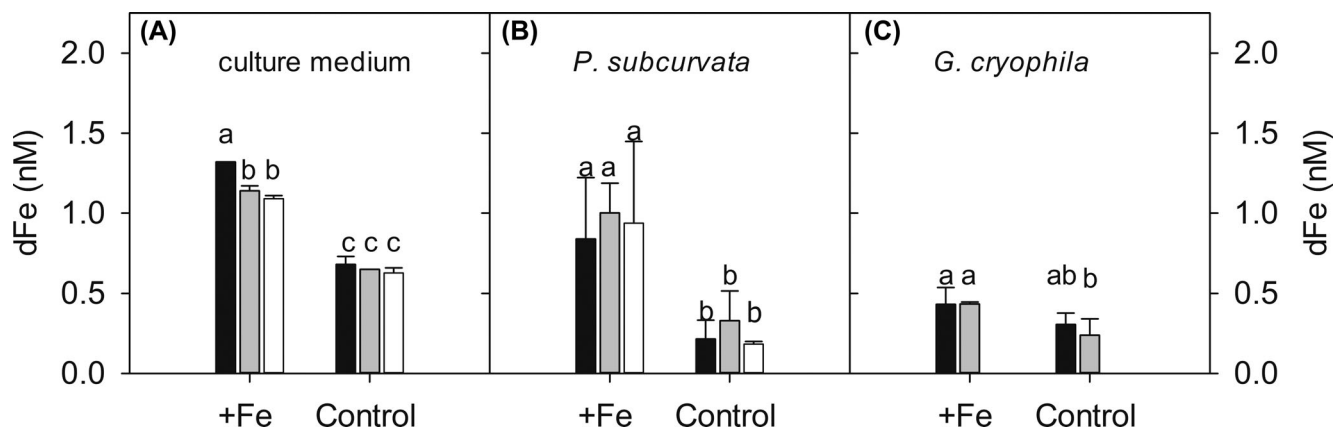

FIGURE 1   Total dissolved Fe (dFe) concentrations of the culture media (A) of the different pCO_2 treatments (400, 900, and 1400) without (Control) and with Fe enrichment (+Fe). Concentrations of dFe were also determined in all incubation bottles of *Pseudo-nitzschia subcurvata* (B) and *Geminigera cryophila* (C) at the end of the experiment. Both cultures were grown under Fe-deplete (Control) and Fe-enriched (+Fe) conditions in combination with 400 (black) or 900 µatm (gray) pCO_2. An additional pCO_2 treatment of 1400 µatm (white) was grown for P. subcurvata. Values represent the mean and SD (culture medium, $n = 2$; incubation bottles, $n = 3$). Significant differences between treatments are indicated by varying lower case letters (post hoc tests, $P < 0.05$)
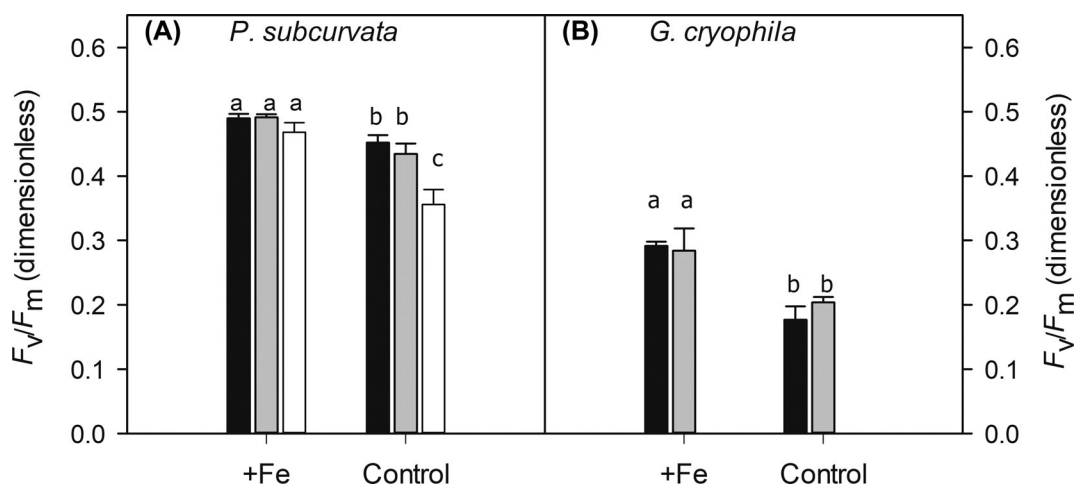

FIGURE 2   The dark-adapted maximum photosystem II quantum yield F_v/F_m for *Pseudo-nitzschia subcurvata* (A) and *Geminigera cryophila* (B) grown under Fe-deplete (Control) and Fe-enriched (+Fe) conditions at different pCO_2 levels: 400 µatm (black), 900 µatm (gray) and 1400 µatm (white, for P. subcurvata only). Values represent the mean and SD ($n = 3$). Significant differences between treatments are indicated by varying lower case letters (post hoc tests, $P < 0.05$)

between 400 and 900, but was significantly reduced by 21% toward 1400 ($P < 0.001$). Lower [dFe] strongly decreased the F_v/F_m for all pCO_2 levels in the diatom (400: $P = 0.01$; 900: $P < 0.001$; 1400:

$P < 0.001$). For the diatom, there was a significant interactive effect of CO_2 and Fe on F_v/F_m, with the lowest value encountered in the 1400-Control treatment ($P = 0.003$). For *G. cryophila* (Figure 2B),
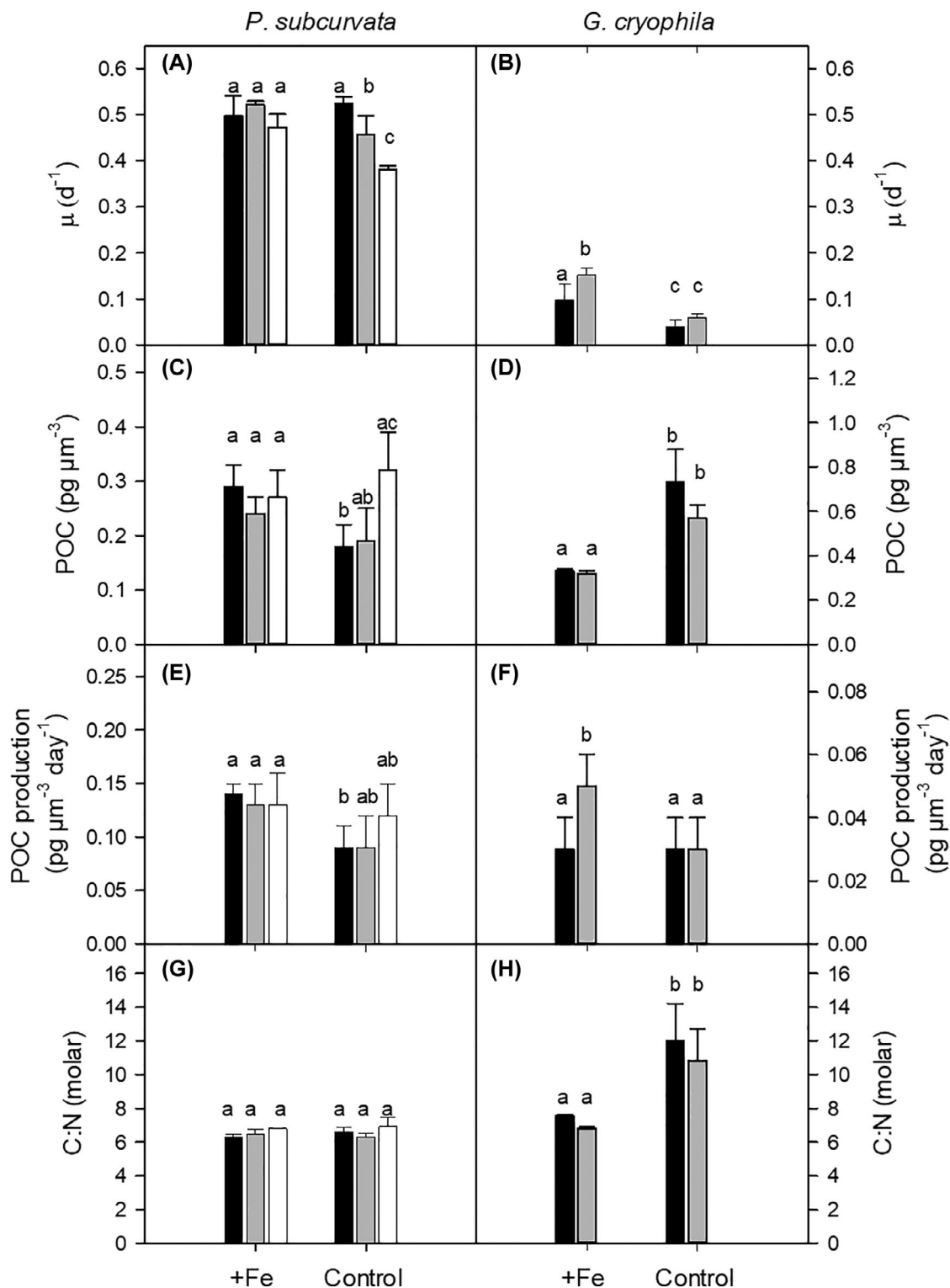

FIGURE 3 Growth rates (A, B), cellular particulate organic carbon (POC) quota normalized to cell volume (C, D), POC production rate normalized to cell volume (E, F) and molar carbon:nitrogen (C:N) ratios (G, H) of *Pseudo-nitzschia subcurvata* (A, C, E, and G) and *Geminigera cryophila* (B, D, F, and H) grown under Fe-deplete (Control) and Fe-enriched (+Fe) conditions at different pCO_2 levels: 400 (black), 900 (grey) and 1400 μatm (white, for *P. subcurvata* only). Values represent the mean and SD ($n = 3$). Significant differences between treatments are indicated by varying lower case letters (post hoc tests, $P < 0.05$)

increasing $p\text{CO}_2$ had no effect on the F_v/F_m for both Fe treatments. A negative Fe-effect was, however, observed for the cryptophyte, wherein F_v/F_m of Control cells was significantly lowered by 40% and 28% in the 400 ($P < 0.001$) and 900 ($P = 0.003$) treatment, respectively.

2.2.3 | Growth and elemental composition

For the +Fe treatments of *P. subcurvata*, no CO_2-effect was observed (Figure 3A), whereas increasing $p\text{CO}_2$ significantly decreased the
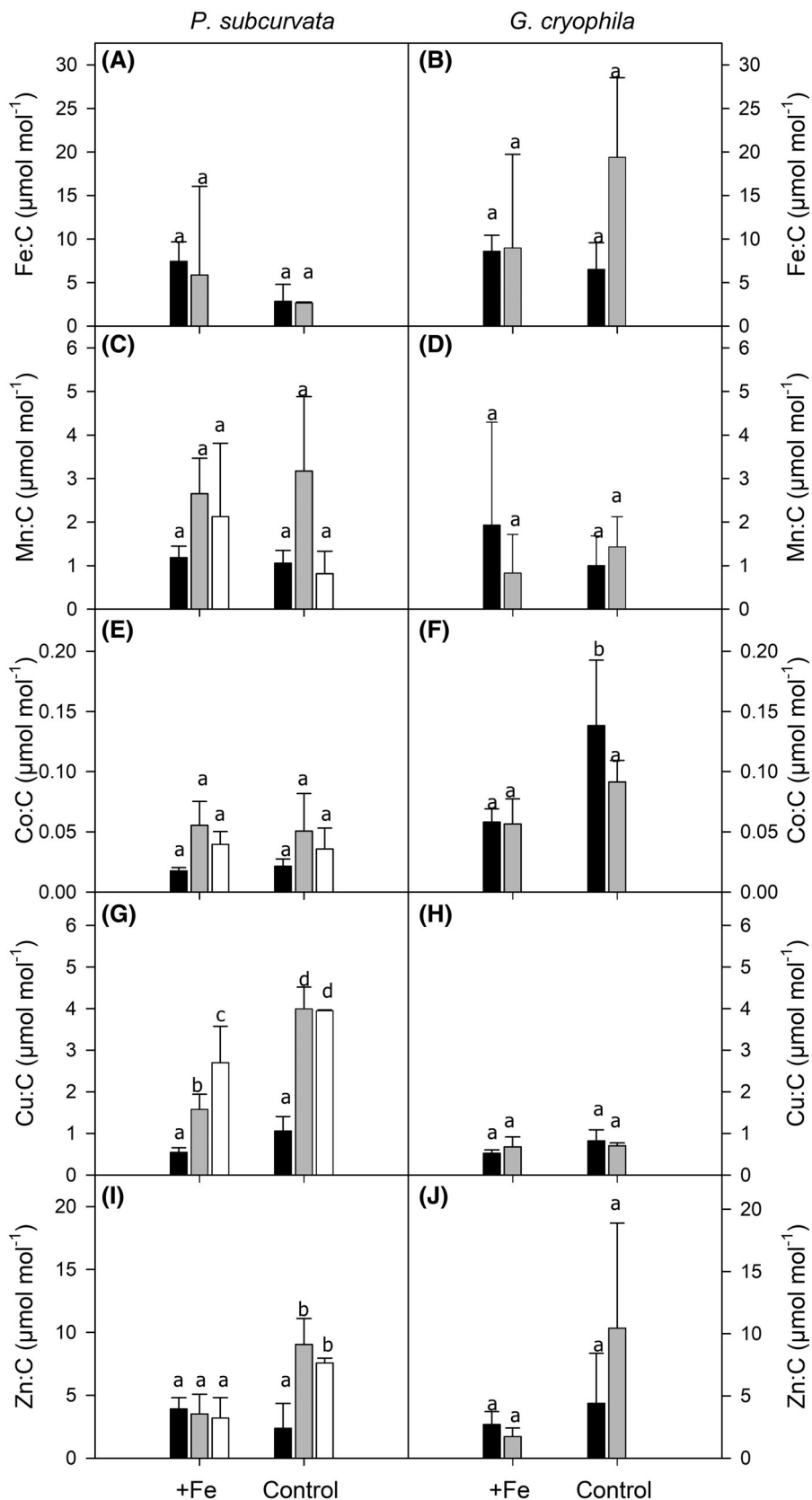

FIGURE 4 Molar trace metal to carbon (TM:C) ratios of *Pseudo-nitzschia subcurvata* (A, C, E, G, and I) and *Geminigera cryophila* (B, D, F, H, and J) grown under Fe-deplete (Control) and Fe-enriched (+Fe) conditions at different $p\text{CO}_2$ levels: 400 (black) and 900 (grey). No Fe quota was measured for the 1400 μatm $p\text{CO}_2$ treatment of *P. subcurvata*. Values represent the mean and SD ($n = 3$). Significant differences between treatments are indicated by varying lower case letters (post hoc tests, $P < 0.05$)

growth rates of the Control cells ($P < 0.001$). Lower [dFe] decreased the growth of *P. subcurvata* by 13% ($P = 0.02$) and 19% ($P = 0.002$) at 900 and 1400, respectively, but not at 400. Hence, there was a significant interactive effect of CO_2 and Fe on the growth rate of

P. subcurvata ($P = 0.01$). For *G. cryophila* (Figure 3B), both significant OA and Fe effects were observed, while the interaction between both factors had no effect on growth. Increasing pCO_2 significantly promoted higher growth rates in the +Fe (54%, $P = 0.012$) but had no

TABLE 2 Cellular quotas (normalized to cell volume) of chlorophyll a (Chl *a*), chlorophyll c_2 (Chl c_2), fucoxanthin (Fuco), diadinoxanthin (Dd) and alloxanthin (Allo) were measured for *Pseudo-nitzschia subcurvata* and *Geminigera cryophila* grown at 400 and 900 µatm pCO_2 in combination with Fe-deplete (Control) or Fe-enriched (+Fe) conditions. An additional pCO_2 treatment of 1400 µatm was grown for *P. subcurvata*. Significant differences between treatments (post hoc tests) are indicated by varying lower case letters in superscript ($P < 0.05$). Values represent the mean and SD ($n = 3$)

| Species	Fe	pCO_2	Chl *a* (fg µm^{-3})	Chl c_2 (fg µm^{-3})	Fuco (fg µm^{-3})	Dd (fg µm^{-3})	Allo (fg µm^{-3})
P. subcurvata	+ Fe	400	4.6 ± 0.7[a]	0.4 ± 0.1[a]	2.3 ± 0.3[a]	0.7 ± 0.1[a]	
P. subcurvata	+ Fe	900	3.1 ± 0.5[b]	0.3 ± 0.0[a]	1.6 ± 0.3[b]	0.4 ± 0.0[b]	
P. subcurvata	+ Fe	1400	3.2 ± 0.7[b]	0.3 ± 0.1[a]	1.8 ± 0.4[ab]	0.4 ± 0.1[b]	
P. subcurvata	Control	400	2.7 ± 0.5[b]	0.3 ± 0.0[a]	1.5 ± 0.3[b]	0.3 ± 0.1[b]	
P. subcurvata	Control	900	2.6 ± 0.2[b]	0.2 ± 0.0[a]	1.4 ± 0.0[b]	0.3 ± 0.1[b]	
P. subcurvata	Control	1400	3.2 ± 0.3[b]	0.3 ± 0.1[a]	1.8 ± 0.2[b]	0.5 ± 0.1[b]	
G. cryophila	+ Fe	400	2.3 ± 0.2[a]	0.4 ± 0.0[a]			1.3 ± 0.1[a]
G. cryophila	+ Fe	900	2.4 ± 0.2[a]	0.3 ± 0.1[a]			1.3 ± 0.1[a]
G. cryophila	Control	400	1.5 ± 0.0[b]	0.2 ± 0.0[b]			1.0 ± 0.0[b]
G. cryophila	Control	900	1.9 ± 0.1[c]	0.3 ± 0.0[ab]			1.2 ± 0.0[c]
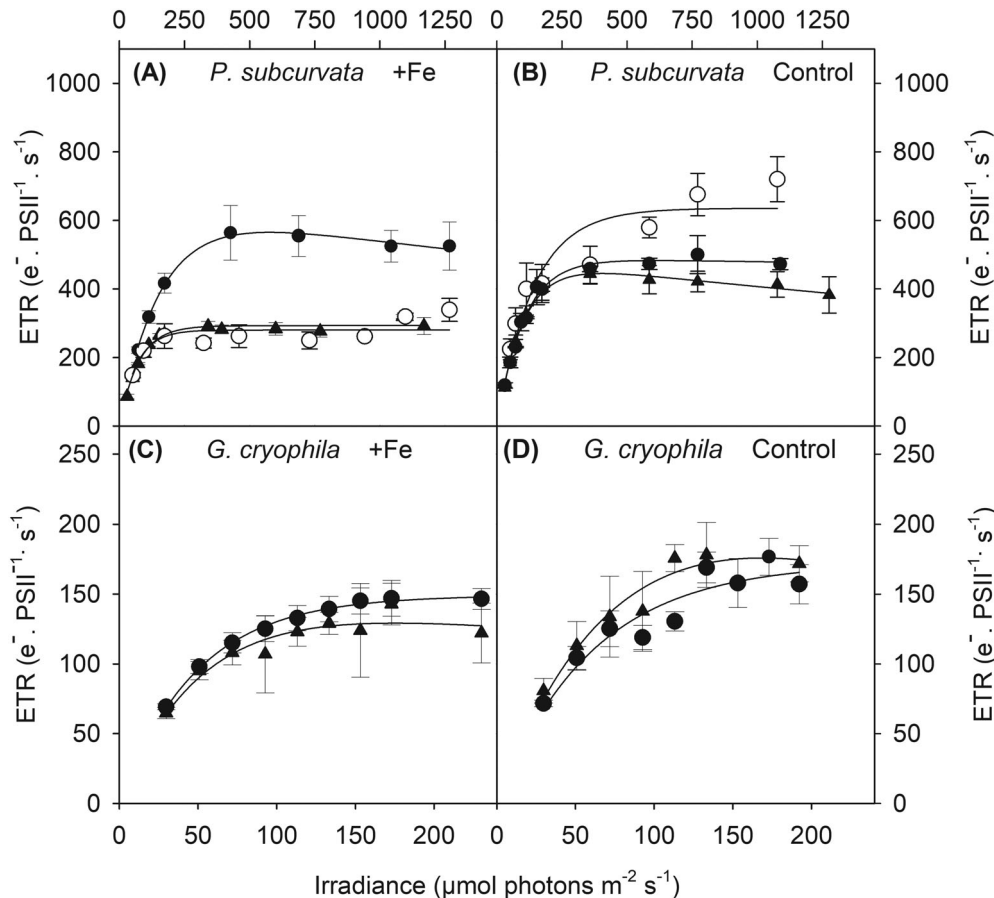
FIGURE 5 Absolute electron transport rates (ETR) were measured in response to increasing irradiance in *Pseudo-nitzschia subcurvata* (A, B) and *Geminigera cryophila* (C, D) grown under Fe-deplete (Control) and Fe-enriched (+Fe) conditions at different pCO_2 levels: 400 µatm (filled circle), 900 µatm (filled triangle) and 1400 µatm (open circle, for *P. subcurvata* only). ETR values show the mean and SD ($n = 3$)

effect in the Control. Lower [dFe] strongly decreased the growth of *G. cryophila* in both pCO_2 treatments ($P < 0.01$).

POC quotas of *P. subcurvata* cells in the +Fe were not affected by OA (Figure 3C). In the Control, POC was similar between 400 and 900, but was enhanced toward 1400. Lower [dFe] decreased the POC quota of *P. subcurvata* by 40% at 400 ($P = 0.015$), while no Fe-effect was observed at 900 and 1400. For *G. cryophila*, no CO_2 effect was evident in both +Fe and Control treatments (Figure 3D). Lower [dFe], however, resulted in a significant increase of the POC quotas by 120% and 75% in the 400 ($P < 0.001$) and 900 treatments ($P = 0.001$), respectively.

In all treatments of the diatom (Figure 3E), no CO_2 effect on POC production rates was observed. Lower [dFe] significantly decreased the POC production rates of *P. subcurvata* by 36% in the 400 treatment ($P = 0.018$) while it had no effect on the other two pCO_2 treatments. In *G. cryophila* (Figure 3F), increasing pCO_2 enhanced the POC production of +Fe cells by 53% ($P = 0.023$), but remained constant in Control cells. With lower [dFe], POC production remained unchanged in the 400 treatment but was decreased by 32% in the 900 treatment ($P = 0.033$).

Compared to *P. subcurvata*, higher C:N ratios were generally determined for *G. cryophila* (Figure 3G, H). Neither CO_2 nor Fe affected C:N ratios of *P. subcurvata*. For *G. cryophila*, increasing pCO_2 did not change the C:N ratio in any Fe treatments, while lower [dFe] resulted in a significant increase in the C:N ratios of the cryptophyte in both pCO_2 treatments ($P = 0.01$).

2.2.4 | Trace metal quotas

Neither OA nor Fe had an effect on the Fe:C, Mn:C, and Co:C ratios of *P. subcurvata* (Figure 4). However, with increasing pCO_2, there was a significant enhancement in the Cu:C ratio of the diatom in both Fe treatments. With lower [dFe], Cu:C ratios increased at 900 ($P < 0.001$) and 1400 ($P = 0.015$), while no change at 400. Zn:C ratios of *P. subcurvata* in the +Fe were not affected by OA, but it was significantly increased in the Control cells between 400 and

900 ($P = 0.003$), but not toward 1400. With lower [dFe], Zn:C ratios of the diatom increased by 150% and 138% at 900 ($P = 0.004$) and 1400 ($P = 0.019$), respectively. In *G. cryophila*, TM:C ratios were more variable than that of the diatom, thus differences between treatments were not significant and difficult to interpret. It was only for the Co:C ratio at 400 pCO_2 that we observed a significant increase in response to lower [dFe] ($P = 0.013$).

2.2.5 | Pigment quotas

In *P. subcurvata*, except for Chl c_2, all pigment quotas of the +Fe cells were decreased from 400 to 900, but with no further change toward 1400 (Table 2). In general, no OA effect was found for the Control. The lowered Fe concentration significantly reduced quotas of Chl a (41%: $P = 0.001$), Fuco (35%: $P = 0.005$), and Dd (52%: $P > 0.001$) when grown at 400 while no Fe-effect was found at 900 and 1400. For *G. cryophila*, with increasing pCO_2, concentrations of Chl a ($P = 0.016$) and Allo ($P = 0.007$) were significantly enhanced, but only in the Control (Table 2). In general, lower [dFe] decreased the pigment concentrations of the cryptophyte at 400 and 900, except for the Chl c_2 quota of cells grown at 900.

2.2.6 | Photophysiological characteristics

The two species showed distinct FLC in response to the different CO_2–Fe treatments (Figure 5). For *P. subcurvata*, a significant interactive effect between CO_2 and Fe on ETR_{max} was found ($P < 0.001$). In the +Fe treatment, ETR_{max} decreased between 400 and 900 ($P = 0.01$), but remained unchanged toward 1400 (Table 3). For the Control, a significant CO_2-dependent increase in ETR_{max} was only observed between 900 and 1400 ($P = 0.006$). Lower [dFe] did not alter the ETR_{max} of *P. subcurvata* cells grown at 400, whereas a strong increase was seen at 900 ($P = 0.003$) and 1400 ($P < 0.001$). In

TABLE 3 Maximum electron transport rates (ETR_{max}), minimum saturating irradiance (I_k), and maximum light utilization efficiency (α) were determined for *Pseudo-nitzschia subcurvata* and *Geminigera cryophila*. Both species were grown under Fe-deplete (Control) and Fe-enriched (+Fe) conditions in combination with 400 and 900 µatm pCO_2. An additional pCO_2 treatment of 1400 µatm was grown for *P. subcurvata*. Values represent the mean and SD ($n = 3$). Significant differences between treatments (post hoc tests) are indicated by varying lower case letters in superscript ($P < 0.05$)

Species	Fe	pCO_2	ETR_{max} (e$^-$ PSII^{-1} s^{-1})	I_k (µmol photons m^{-2} s^{-1})	α (rel. unit)
P. subcurvata	+ Fe	400	565 ± 68[a]	140 ± 15[a]	4.1 ± 0.2[a]
P. subcurvata	+ Fe	900	293 ± 6[b]	73 ± 5[b]	4.0 ± 0.2[a]
P. subcurvata	+ Fe	1400	275 ± 18[b]	59 ± 7[b]	4.7 ± 0.9[a]
P. subcurvata	Control	400	519 ± 63[a]	114 ± 9[c]	4.6 ± 0.2[a]
P. subcurvata	Control	900	445 ± 33[a]	90 ± 2[b]	4.9 ± 0.4[a]
P. subcurvata	Control	1400	673 ± 74[c]	142 ± 24[d]	5.0 ± 1.4[a]
G. cryophila	+ Fe	400	147 ± 8[a]	49 ± 2[a]	3.0 ± 0.1[a]
G. cryophila	+ Fe	900	137 ± 8[a]	46 ± 7[a]	3.0 ± 0.4[a]
G. cryophila	Control	400	170 ± 18[ab]	62 ± 5[b]	2.8 ± 0.2[a]
G. cryophila	Control	900	175 ± 18[b]	54 ± 4[ab]	3.3 ± 0.6[a]

G. cryophila, increasing pCO$_2$ had no effect on ETR$_{max}$ in both Fe treatments. Lower [dFe], however, led to a 28% increase in ETR$_{max}$, but only when grown at 900 ($P = 0.009$). Similar to ETR$_{max}$, I_k in *P. subcurvata* was strongly influenced by the different CO$_2$–Fe treatments (Table 3). In the +Fe, I_k was highest in the 400 treatment, while no significant difference in I_k was observed between 900 and 1400. In the Control, there was a decrease of I_k (21%) from 400 to 900 ($P = 0.04$), while from 900 to 1400, a 58% increase was observed ($P < 0.001$). In *P. subcurvata*, lower [dFe] caused a minor decrease in I_k at 400 ($P = 0.028$), had no effect at 900 and enhanced I_k at 1400 ($P < 0.001$). For the cryptophyte, no CO$_2$-dependent effects on I_k were observed. In response to lower [dFe], I_k increased by 27% at 400 ($P = 0.012$) while there was no change at 900. For both species, α was neither altered by CO$_2$ nor by Fe availability (Table 3).

During the FLC, both species exhibited higher NPQ values with increasing irradiance in all treatments (Figure 6). For the +Fe treatment of *P. subcurvata*, no CO$_2$-dependent differences were seen in NPQ. In the Control, a CO$_2$-effect was observed wherein at irradiances >1000 μmol photons m^{-2} s^{-1}, lowest and highest NPQ values were encountered in the 400 and 1400 treatments, respectively. Again, at irradiances >1000 μmol photons m^{-2} s^{-1}, lower [dFe] resulted in an increase in NPQ but only for the 1400 treatment of the diatom. In the case of *G. cryophila*, neither a CO$_2$ nor Fe effect on NPQ was observed.

3 | DISCUSSION

3.1 | Compared to the diatom, growth of the cryptophyte was drastically impacted by low Fe supply at ambient pCO$_2$

The Control treatments of both species displayed common photophysiological characteristics of Fe-stressed cells (Alderkamp et al., 2012; Koch et al., 2018; Strzepek et al., 2011, 2012; Trimborn et al., 2019a) such as reduced F_v/F_m values (Figure 2A, B) accompanied by enhanced functional absorption cross-section of PSII (σ$_{PSII}$; Table S2). The increase in σ$_{PSII}$ enabled the Fe-limited cells to ensure similar light usage (Ryan-Keogh et al., 2012). In contrast, the low Fe supply differently affected the growth of the two species under ambient pCO$_2$, as growth remained the same in *P. subcurvata* while it was significantly reduced in *G. cryophila*.

Although F_v/F_m was decreased in the Control relative to the +Fe under ambient pCO$_2$ (Figure 2A), the diatom maintained similar high growth rates (0.52±0.01 d^{-1}, Figure 3A). Similarly, for various temperate oceanic *Pseudo-nitzschia* isolates, substantial reductions in the photochemical yield were found despite having little or no change in growth (Marchetti et al., 2006). The authors explained that growth and photophysiology are usually decoupled in oceanic *Pseudo-nitzschia* species and that under Fe limitation, oceanic species have a low Fe requirement to achieve rapid growth. Indeed, our *P. subcurvata*
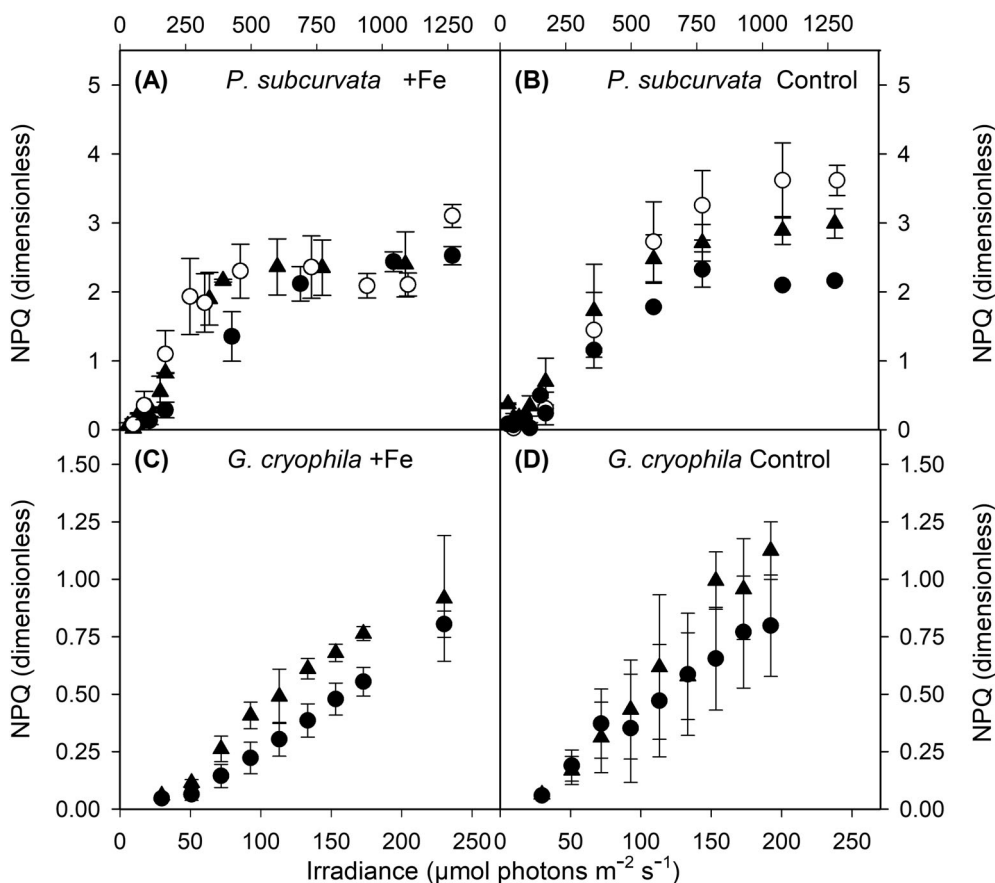

FIGURE 6 Nonphotochemical quenching (NPQ) was measured in response to increasing irradiance in *Pseudo-nitzschia subcurvata* (A, B) and *Geminigera cryophila* (C, D) grown under Fe-deplete (Control) and Fe-enriched (+Fe) conditions at different pCO$_2$ levels: 400 μatm (filled circle), 900 μatm (filled triangle) and 1400 μatm (open circle, for *P. subcurvata* only). NPQ values show the mean and SD ($n = 3$)

was isolated from open waters of the Southern Ocean (49° S) and exhibited lower Fe:C ratios (2.85 µmol mol^{-1}, Figure 4A) compared to that of the *P. subcurvata* strain isolated from the sea ice edge in the Ross Sea (10-50 Fe:C µmol mol^{-1}; Zhu et al., 2016) and the ones measured in temperate coastal *Pseudo-nitzschia* species (5-11 Fe:C µmol mol^{-1}; Marchetti et al., 2006). Oceanic *Pseudo-nitzschia* species also have the ability to carry out luxury Fe uptake and store this surplus in the Fe storage protein ferritin (Cohen et al., 2018; Lampe et al., 2018; Marchetti et al., 2006, 2017; Sunda & Huntsman, 1995). Although not statistically significant, our Control cells had a lower intracellular Fe content than the +Fe cells under ambient pCO_2 (Figure 4A). This may suggest that the Control cells may have used their internal Fe pool, allowing them to keep growth constant relative to the +Fe cells. When comparing the growth rate of our *P. subcurvata* in both Fe treatments under ambient pCO_2 (+Fe: 0.50 ± 0.04 d^{-1}; Control: 0.52 ± 0.01 d^{-1}, Figure 3A) with the one reported in the same strain grown under ample supply of Fe (μ = 0.9 d^{-1}; 12 µM Fe, Trimborn et al., 2013) and that in the study of Moreno et al. (2018) (μ = 0.6 d^{-1}; 2.7 nM Fe), it becomes evident that our *P. subcurvata* cultures were already experiencing Fe stress in our +Fe treatments. Hence, the +Fe conditions applied here (1.2 nM Fe) were already Fe-limiting for *P. subcurvata*.

Compared to the diatom, F_v/F_m and growth of the cryptophyte *G. cryophila* were much more strongly affected by lower [dFe] under ambient pCO_2. The cryptophyte almost stopped growing in our Control treatments, dividing only at 0.05 d^{-1}. Comparing our growth rate of *G. cryophila* under ambient pCO_2 in the +Fe treatment (1.2 nM Fe, μ = 0.10 ± 0.03 d^{-1}, Figure 3B) with the values determined in the same strain under high (Aquil medium, 2 µM Fe, Koch and Trimborn (2019) and very high (12 µM, Trimborn et al., 2019b) Fe concentrations, in this study growth was already strongly reduced. To verify this, we grew the cryptophyte at 2 nM Fe, and indeed, we found a significant enhancement in growth (0.24 d^{-1}, data not shown). In fact, the exposure of *G. cryophila* to our Control conditions (0.6 nM Fe, Figure 1A) strongly amplified the effect of Fe limitation, with the Control cells exhibiting stronger reductions in F_v/F_m, growth and cellular pigment concentrations (Chl *a*, Chl c_2, and Allo) as well as higher I_k (Figures 2B and 3B, Tables 2 and 3). Indeed, the Control conditions were more stressful for the cryptophyte than the +Fe conditions under ambient pCO_2.

Fe has a crucial role in the electron transport chain as it is an important component of the photochemical reaction centers (Behrenfeld & Milligan, 2012; Strzepek & Harrison, 2004). It is a common response of phytoplankton to reduce its maximum quantum yield (F_v/F_m) as well as its photosynthetic ETRs under Fe limitation (Koch & Trimborn, 2019; Petrou et al., 2014). In this study, while the maximum ETRs and NPQ of the diatom remained the same between the +Fe and Control (Table 3, Figures 5 and 6), POC production was, however, significantly reduced in the Control cells (Figure 3E), suggesting the utilization of alternative electron sinks other than solely undergoing photosynthetic carbon assimilation. Lower [dFe] also caused an earlier onset of light saturation in the diatom, as indicated by the decrease in I_k in the Control relative to the +Fe treatment (Table 3). To potentially counteract this and diminish light absorption, the concentration of light harvesting pigments (Chl *a* and Fuco) (Table 2), as well as the cellular concentration of functional PSII reaction centers ([RCII]) and the connectivity between PSII (*P*) were reduced in the Control (Table S2). These adjustments enabled *P. subcurvata* to cope well with short-term light stress, as shown by the similar high F_v/F_m recovery (% of the ratio of F_v/F_m determined before and after the FLC) between the +Fe and Control treatments. Overall, even though fast growth was achieved in both Control and +Fe cells, all results together (F_v/F_m, σ_{PSII}, POC, PON, pigments) point toward the fact that the Control conditions were more stressful for the diatom than the +Fe conditions under ambient pCO_2.

Similar to *P. subcurvata*, the cryptophyte also exhibited high tolerance to short-term light stress as it had similar high F_v/F_m recovery values in both Control and +Fe cells (Table S2). Moreover, *G. cryophila* maintained similar POC production rates between the +Fe and Control under ambient pCO_2 (Figure 3F). This unchanged POC production of the Control cells was a consequence of a more enhanced cellular POC buildup while cell division almost stopped (Figure 3B, D, F). At the same time, PON quota remained unchanged in Control versus +Fe cells (Figure S1B). Consequently, the C:N ratio was enhanced in the cryptophyte Control (Figure 3H), which was likely the result of the Fe-limited cells acquiring excess carbon, as evident in the significant increase of POC quota of the Control (Figure 3D). Hence, the Control cells of *G. cryophila* may have prioritized carbon fixation over cell division, as previously observed for the same species under Fe limitation (Koch & Trimborn, 2019) and the Fe-limited diatom *Thalassiosira antarctica* (Andrew et al., 2019). All these photophysiological adjustments of the cryptophyte suggest that Control cells became saturated at higher light intensities, thus requiring higher light to sustain the same rate of POC production (Figure 3F).

Previous studies have shown an increase in cellular Cu concentration of several phytoplankton species in response to Fe limitation (Annett et al., 2008; Guo et al., 2012; Koch & Trimborn, 2019; Maldonado et al., 2006; Semeniuk et al., 2009; Wells et al., 2005). This is because Cu is needed in Fe-reductases and multicopper oxidases, being thus important components of the high-affinity Fe uptake system (Behnke & LaRoche, 2020; Maldonado et al., 2006). This increase in Cu quotas with low Fe supply was, however, not found in *G. cryophila* (Figure 4H) since the Cu:C ratio remained unchanged irrespective of Fe availability under ambient pCO_2. This agrees with the observations of Koch and Trimborn (2019), and further fits well with the observation that the marine cryptophyte *Guillardia theta* did not possess the gene encoding for the Cu-containing enzyme plastocyanin (Blaby-Haas & Merchant, 2017). Under Fe limitation, oceanic diatoms (Peers & Price, 2006) are commonly observed to substitute the Fe-requiring cytochrome c6 with plastocyanin in the electron transport chain (Behrenfeld & Milligan, 2012; Castell et al., 2021; Raven et al., 1999). Moreover, similar to *P. subcurvata* (Moreno et al., 2018), two different cryptophyte species did not have genes encoding Fe-reductases and multicopper oxidases (Behnke & LaRoche, 2020; Curtis et al., 2012), indicating the inability of both species for Cu-dependent high-affinity Fe uptake (Behnke &

LaRoche, 2020; Moreno et al., 2018). Taken together these observations may explain why the cryptophyte was more drastically impacted than the diatom under low Fe supply.

Overall, our results clearly show that under ambient pCO_2, low Fe supply was stressful for both the diatom and the cryptophyte, but with the diatom coping much better with these conditions. The diatom underwent physiological adjustments, which on the one hand, led to reduced carbon buildup and the need for dissipation of excess light energy, but enabling it to sustain high growth rates on the other hand. In contrast, low Fe was highly detrimental for the cryptophyte as it almost stopped dividing.

3.2 | OA together with Fe supply was beneficial for *G. cryophila*, but not for *P. subcurvata*

A meta-analysis on OA effects on SO phytoplankton (Hancock et al., 2018) revealed that Antarctic phytoplankton is generally unaffected by pCO_2 levels below 1000 μatm, with negative effects on physiology becoming evident only at higher pCO_2 levels. In line with the results for the same (Trimborn et al., 2013) and another (Zhu et al., 2017) *P. subcurvata* strain, an increase in pCO_2 up to 1400 μatm did not alter growth or POC production of *P. subcurvata* under +Fe conditions (Figure 3A,E). We observed, however, OA-dependent changes in its photoacclimation. Even though F_v/F_m and σ_{PSII} remained the same between 400 and 900 μatm pCO_2 (Figure 2A, Table S2), [RCII] (Table S2), ETR_{max}, I_k and pigment concentration (Chl *a*, Fuco and Dd) were significantly reduced (Tables 2 and 3, Figure 5), suggesting that electron transport was downregulated, as previously observed (Trimborn et al., 2017a). Calculations of photosynthetic electron transport using the model by Kroon and Thoms (2006) revealed that the higher the rates of electron consumption in upstream metabolic reactions, such as CO_2 fixation by RubisCO, the more pronounced is the decline of the ATP synthesis rate relative to the rate of NADPH synthesis (Trimborn et al., 2017a). Consequently, in this study, downregulation of ETRs can preclude ATP limitation under OA and Fe-enrichment. Furthermore, we observed a highly significant OA-dependent increase in the Cu:C ratio of *P. subcurvata* cells in the +Fe treatments (390 vs. 900: 187%; 390 vs. 1400: 391%, Figure 4G). This was unexpected, as enhanced Cu:C ratios are usually found only in response to Fe limitation and not to OA. For diatoms, the low carbonate concentration present under high pCO_2 was identified to hamper the phytotransferrin-dependent high-affinity Fe uptake (McQuaid et al., 2018). Indeed, the gene encoding for the ferric Fe-concentrating protein ISIP2a (phytotransferin) was found in *P. subcurvata* (Moreno et al., 2018). Perhaps, due to the hampered Fe uptake under increasing pCO_2, the diatom may have potentially switched from using cytochrome c6 to plastocyanin instead, thus increasing the Cu:C ratios. The potentially impacted phytotransferrin-based Fe uptake pathway of the diatom under OA (i.e. low carbonate concentration) may explain why *P. subcurvata* did not benefit from OA even under higher Fe supply, as growth and POC production remained unchanged.

In comparison to the diatom, growth and POC production of the cryptophyte were significantly promoted between 400 and 900 μatm pCO_2 under +Fe, suggesting that *G. cryophila* benefitted from lower energy requirements under OA. Similar observations were made for the same cryptophyte strain grown under OA and high light (200 μmol photons m^{-2} s^{-1}, Trimborn et al., 2019b). In contrast to the diatom, OA did not alter the photoacclimation status of the cryptophyte under +Fe conditions, with no changes in cellular concentrations of the light harvesting pigments (Chl *a*, Chl c$_2$, and Allo) and photophysiolgy (F_v/F_m, σ_{PSII}, ETR_{max}, and I_k). The slight increase in NPQ (Figure 6C) suggests that excess light energy was dissipated as heat to prevent overexcitation, enabling the cryptophyte to cope well with high light stress in the short term (F_v/F_m recovery of >90%, Table S2). Moreover, ratios of Fe:C as well as of the other TMs (Mn, Co, Cu, and Zn) remained constant between 400 and 900 μatm pCO_2 (Figure 4), which may indicate that TM requirements of the cryptophyte did not change under OA and high Fe supply. As in Trimborn et al.(2019b), *G. cryophila* benefited from OA under higher Fe availability.

3.3 | The diatom coped better with low Fe supply and OA than the cryptophyte, but required adjustments in its photophysiology

For *G. cryophila*, in contrast to the +Fe treatment, Control cells were so strongly Fe limited that increasing pCO_2 did no longer have any effect in most of the investigated physiological parameters (growth, POC production, TM:C ratios, photophysiology, Figures 3 and 4, Table 3). This indicates that Fe limitation alone was the main controlling factor on the cryptophyte. In comparison to the cryptophyte, increasing pCO_2 in combination with low Fe supply synergistically reduced the growth rates of *P. subcurvata* (Figure 3A). Simultaneously, POC production rates, cellular pigment pools (Chl *a*, Chl c$_2$, Fuco, and Dd) (Figure 3E, Table 2) and the number of functional RCII remained the same (Table S2). However, ETR_{max} was significantly enhanced under these conditions, which may suggest saturation of the Calvin Cycle and the need for alternative electron cycling. Accordingly, we observed highest NPQ values in the 1400 pCO_2-Control treatment (Figure 6B), indicating that not all light energy was channeled downstream and partially dissipated as heat. Control cells may have also operated alternative electron pathways (Behrenfeld & Milligan, 2012) such as cyclic electron transport around PSII (Prasil et al., 1996) and plastid terminal oxidases (Mackey et al., 2008). In previous studies, exposure to either OA or Fe limitation alone was found to increase the production of reactive oxygen species in some phytoplankton species (Allen et al., 2008; Wu et al., 2021). For *P. subcurvata*, one may speculate whether the combined effect of OA and low Fe supply may have also led to higher oxidative stress, most pronounced in the 1400 pCO_2-Control treatment. In line with this, highest Cu:C and Zn:C ratios were observed in the 900 and 1400 pCO_2-Control treatments (Figure 4G), indicating that the diatom may have utilized Cu/Zn superoxide dismutase (Cu/Zn SOD) to counteract the formation of reactive oxygen species (Alscher et al., 2002). Hence, the low Fe availability amplified the negative effects of OA in *P. subcurvata*, hampering linear electron transport and thus increasing the need to dissipate the excess light energy (NPQ, alternative electron sinks). The latter

mechanisms were probably insufficient and potentially increased the formation of reactive oxygen species, impacting the physiological performance of the diatom.

3.4 | Ecological implications

While diatoms form blooms in both open ocean and coastal regions of the SO (Smetacek et al., 2012), high abundances of cryptophytes are mainly observed in coastal SO waters (Brown et al., 2021; Moline et al., 2004; Montes-Hugo et al., 2009). In this study, we provide evidence that cryptophytes such as *G. cryophila* cannot cope well with low Fe concentrations, which are typical for open SO waters. Our findings suggest that low Fe conditions are detrimental for *G. cryophila*, as it almost stopped growing. The reason for this could be that cryptophytes lack the Cu-dependent high-affinity Fe uptake (Behnke & LaRoche, 2020) as well as the capability to substitute cytochrome c6 with plastocyanin. This could explain why cryptophytes mainly occur in coastal waters, which have an ample supply of Fe. In comparison, the oceanic diatom *P. subcurvata* relied on an efficient physiological machinery to cope with low Fe concentration, including low Fe requirements and potentially substituting cytochrome c6 with plastocyanin.

In the future, both groups will need to deal with high CO_2 conditions, with different consequences for their occurrence in Fe-poor and -rich SO waters. In regions with high Fe supply, such as coastal SO waters, high pCO_2 levels could be beneficial for the cryptophyte, displaying elevated rates of growth and POC production, while the diatom would not benefit from OA. The reason for this could be the impacted phytotransferrin-based Fe uptake pathway of the diatom under OA (i.e. low carbonate concentration). In future acidified Fe-poor waters, the overall physiological performance of *P. subcurvata* would be strongly compromised as the low Fe availability amplified the negative effects of OA, in particular impacting its photoacclimation. Overall, our study indicates that Fe availability is a strong modulator of the overall effect imposed by OA on SO phytoplankton, with different implications on the occurrence of cryptophytes and diatoms in the future.

AUTHOR CONTRIBUTION

Scarlett Trimborn conceived and designed the research. Marianne G. Camoying performed the research. Jana K. Geuer analyzed the DA samples and assisted during harvests. Marianne G. Camoying analyzed the data as well as performed the interpretation of data together with Scarlett Trimborn and Silke Thoms. Boris P. Koch contributed lab materials/reagents and analysis tools needed in the study. Marianne G. Camoying, Scarlett Trimborn and Silke Thoms wrote the manuscript with critical feedback from Jana K. Geuer, Kai Bischof and Boris P. Koch. All authors approved the submitted version.

ORCID
Marianne G. Camoying https://orcid.org/0000-0002-4180-7850

REFERENCES

Alderkamp, A.C., Kulk, G., Buma, A.G.J., Visser, R.J., Van Dijken, G.L., Mills, M. et al. (2012) The effect of iron limitation on the photophysiology of *Phaeocystis antarctica* (Prymnesiophyceae) and *Fragilariopsis cylindrus* (Bacillariophyceae) under dynamic irradiance. *Journal of Phycology*, 48, 45–59.

Allen, A., LaRoche, J., Maheswari, U., Lommer, M., Schauer, N., Lopez, P. et al. (2008) Whole-cell response of the pennate diatom *Phaeodactylum tricornutum* to iron starvation. *Proceedings of the National Academy of Sciences of the United States of America*, 105, 10438–10443.

Almandoz, G.O., Ferreyra, G.A., Schloss, I.R., Dogliotti, A.I., Rupolo, V., Paparazzo, F.E. et al. (2008) Distribution and ecology of *Pseudo-nitzschia* species (Bacillariophyceae) in surface waters of the Weddell Sea (Antarctica). *Polar Biology*, 31, 429–442.

Alscher, R.G., Erturk, N. & Heath, L.S. (2002) Role of superoxide dismutases (SODs) in controlling oxidative stress in plants. *Journal of Experimental Botany*, 53, 1331–1341.

Andrew, S.M., Morell, H.T., Strzepek, R.F., Boyd, P.W. & Ellwood, M.J. (2019) Iron availability influences the tolerance of Southern Ocean phytoplankton to warming and elevated irradiance. *Frontiers in Marine Science*, 6, 1–12.

Annett, A.L., Lapi, S., Ruth, T.J. & Maldonado, M.T. (2008) The effects of Cu and Fe availability on the growth and Cu:C ratios of marine diatoms. *Limnology and Oceanography*, 53, 2451–2461.

de Baar, H.J.W., Bathmannt, U., Smetacek, V., Löscher, B.M. & Veth, C. (1995) Importance of iron for plankton blooms and carbon dioxide drawdown in the Southern Ocean. *Nature*, 373, 412–415.

Behnke, J. & LaRoche, J. (2020) Iron uptake proteins in algae and the role of Iron Starvation-Induced Proteins (ISIPs). *European Journal of Phycology*, 55, 339–360.

Behrenfeld, M.J. & Milligan, A.J. (2012) Photophysiological expressions of iron stress in phytoplankton. *Annual Review of Marine Science*, 5, 217–246.

Blaby-Haas, C.E. & Merchant, S.S. (2017) Regulating cellular trace metal economy in algae. *Current Opinion in Plant Biology*, 39, 88–96.

Brown, M.S., Bowman, J.S., Lin, Y., Feehan, C.J., Moreno, C.M., Cassar, N. et al. (2021) Low diversity of a key phytoplankton group along the West Antarctic Peninsula. *Limnology and Oceanography*, 66, 2470–2480.

Castell, C., Bernal-bayard, P. & Hervás, M. (2021) The heterologous expression of a plastocyanin in the diatom *Phaeodactylum tricornutum* improves cell growth under iron- deficient conditions. *Physiologia Plantarum*, 171, 277–290.

Coad, T., McMinn, A., Nomura, D. & Martin, A. (2016) Effect of elevated CO_2 concentration on microalgal communities in Antarctic pack ice. *Deep Sea Research Part II: Topical Studies in Oceanography*, 131, 160–169.

Cohen, N.R., Mann, E., Stemple, B., Moreno, C.M., Rauschenberg, S., Jacquot, J. et al. (2018) Iron storage capacities and associated ferritin gene expression among marine diatoms. *Limnology and Oceanography*, 63, 1677–1691.

Curtis, B.A., Tanifuji, G., Burki, F., Gruber, A., Irimia, M., Maruyama, S. et al. (2012) Algal genomes reveal evolutionary mosaicism and the fate of nucleomorphs. *Nature*, 492, 59–65.

Cutter, G.A., Casciotti, K., Croot, P., Geibert, W., Heimbürger, L.E., Lohan, M. et al. (2017) *Sampling and Sample-handling Protocols for GEOTRACES Cruises*. Toulouse, France: GEOTRACES International Project Office, 139 pp.

Davidson, A.T., McKinlay, J., Westwood, K., Thomson, P., van den Enden, R., de Salas, M. et al. (2016) Enhanced CO_2 concentrations change the structure of Antarctic marine microbial communities. *Marine Ecology Progress Series*, 552, 93–113.

Dickson, A.G. & Millero, F.J. (1987) A comparison of the equilibrium constants for the dissociation of carbonic acid in seawater media. *Deep Sea Research Part A: Oceanographic Research Papers*, 34, 1733–1743.

Donahue, K., Klaas, C., Dillingham, P.W. & Hoffmann, L.J. (2019) Combined effects of ocean acidification and increased light intensity on natural phytoplankton communities from two Southern Ocean water masses. *Journal of Plankton Research*, 41, 30–45.

Feng, Y., Hare, C.E., Rose, J.M., Handy, S.M., DiTullio, G.R., Lee, P.A. et al. (2010) Interactive effects of iron, irradiance and CO_2 on Ross Sea phytoplankton. *Deep Sea Research Part I: Oceanographic Research Papers*, 57, 368–383.

Garibotti, I.A. & Ferrario, M.E. (2005) Annually recurrent phytoplanktonic assemblages during summer in the seasonal ice zone west of the Antarctic Peninsula (Southern Ocean). *Deep-Sea Research*, 52, 1823–1841.

Garibotti, I.A., Vernet, M., Kozlowski, W.A. & Ferrario, M.E. (2003) Composition and biomass of phytoplankton assemblages in coastal Antarctic waters: a comparison of chemotaxonomic and microscopic analyses. *Marine Ecology Progress Series*, 247, 27–42.

Genty, B., Briantais, J.M. & Baker, N.R. (1989) The relationship between the quantum yield of photosynthetic electron transport and quenching of chlorophyll fluorescence. *Biochimica et Biophysica Acta*, 990, 87–92.

Gerringa, L.J.A., De Baar, H.J.W. & Timmermans, K.R. (2000) A comparison of iron limitation of phytoplankton in natural oceanic waters and laboratory media conditioned with EDTA. *Marine Chemistry*, 68, 335–346.

Geuer, J.K., Trimborn, S., Koch, F., Brenneis, T., Krock, B. & Koch, B.P. (2020) Dissolved domoic acid does not improve growth rates and iron content in iron-stressed *Pseudo-Nitzschia subcurvata*. *Frontiers in Marine Science*, 7, 478.

Greene, R.M., Geider, R.J. & Falkowski, P.G. (1991) Effect of iron limitation on photosynthesis in a marine diatom. *Limnology and Oceanography*, 36, 1772–1782.

Greene, R.M., Geider, R.J., Kolber, Z. & Falkowski, P.G. (1992) Iron-induced changes in light harvesting and photochemical energy conversion processes in eukaryotic marine algae. *Plant Physiology*, 100, 565–575.

Guo, J., Lapi, S., Ruth, T.J. & Maldonado, M.T. (2012) The effects of iron and copper availability on the copper stoichiometry of marine phytoplankton. *Journal of Phycology*, 48, 312–325.

Hancock, A.M., Davidson, A.T., Mckinlay, J., Mcminn, A., Schulz, K.G. & van den Enden, R.L. (2018) Ocean acidification changes the structure of an Antarctic coastal protistan community. *Biogeosciences*, 15, 2393–2410.

Hassler, C.S. & Schoemann, V. (2009) Discriminating between intra- and extracellular metals using chemical extractions: an update on the case of iron. *Limnology and Oceanography: Methods*, 7, 479–489.

Heiden, J.P., Völkner, C., Jones, E.M., van de Poll, W.H., Buma, A.G., Meredith, M. et al. (2019) Impact of ocean acidification and high solar radiation on productivity and species composition of a late summer phytoplankton community of the coastal Western Antarctic Peninsula. *Limnology and Oceanography*, 64, 1716–1736.

Henley, S.F., Schofield, O.M., Hendry, K.R., Schloss, I., Steinberg, D., Moffat, C. et al. (2019) Variability and change in the west Antarctic Peninsula marine system: research priorities and opportunities. *Progress in Oceanography*, 173, 208–237.

Hillebrand, H., Dürselen, C.D., Kirschtel, D., Pollingher, U. & Zohary, T. (1999) Biovolume calculation for pelagic and benthic microalgae. *Journal of Phycology*, 35, 403–424.

Hoogstraten, A., Peters, M., Timmermans, K.R. & De Baar, H.J.W. (2012) Combined effects of inorganic carbon and light on *Phaeocystis globosa* Scherffel (Prymnesiophyceae). *Biogeosciences*, 9, 1885–1896.

Hoppe, C.J.M., Hassler, C.S., Payne, C.D., Tortell, P.D., Rost, B. & Trimborn, S. (2013) Iron limitation modulates ocean acidification effects on Southern Ocean phytoplankton communities. *PLoS One*, 8, e79890. https://doi.org/10.1371/journal.pone.0079890

Intergovernmental Panel on Climate Change. (2014) In: Pachauri, R.K. & Meyer, L.A. (Eds.) *Synthesis Report. Contribution of Working Groups I, II and III to the Fifth Assessment Report of the Intergovernmental Panel on Climate Change*. Geneva, Switzerland: Intergovernmental Panel on Climate Change.

Kerr, R., Goyet, C., da Cunha, L.C., da Cunha, L., Orselli, I., Lencina-Avila, J. et al. (2018) Carbonate system properties in the Gerlache Strait, Northern Antarctic Peninsula (February 2015): II. Anthropogenic CO_2 and seawater acidification. *Deep Sea Research Part II: Topical Studies in Oceanography*, 149, 182–192.

Klunder, M.B., Laan, P., Middag, R., De Baar, H.J.W. & Van Ooijen, J.C. (2011) Dissolved iron in the Southern Ocean (Atlantic sector). *Deep Sea Research Part II: Topical Studies in Oceanography*, 58, 2678–2694.

Klunder, M.B., Laan, P., De Baar, H.J.W., Middag, R., Neven, I. & Van Ooijen, J.C. (2014) Dissolved Fe across the Weddell Sea and Drake Passage: Impact of DFe on nutrient uptake. *Biogeosciences*, 11, 651–669.

Koch, F. & Trimborn, S. (2019) Limitation by Fe, Zn, Co, and B_{12} results in similar physiological responses in two Antarctic phytoplankton species. *Frontiers in Marine Science*, 6, 514.

Koch, F., Beszteri, S., Harms, L. & Trimborn, S. (2018) The impacts of iron limitation and ocean acidification on the cellular stoichiometry, photophysiology, and transcriptome of *Phaeocystis antarctica*. *Limnology and Oceanography*, 64, 357–375.

Kolber, Z.S., Prášil, O. & Falkowski, P.G. (1998) Measurements of variable chlorophyll fluorescence using fast repetition rate techniques: Defining methodology and experimental protocols. *Biochimica et Biophysica Acta*, 1367, 88–106.

Kroon, B.M.A. & Thoms, S. (2006) From electron to biomass: A mechanistic model to describe phytoplankton photosynthesis and steady-state growth rates. *Journal of Phycology*, 42, 593–609.

Lampe, R.H., Mann, E.L., Cohen, N.R., Till, C.P., Thamatrakoln, K., Brzenzinski, M.A. et al. (2018) Different iron storage strategies among bloom-forming diatoms. *Proceedings of the National Academy of Sciences of the United States of America*, 115, E12275–E12284.

van Leeuwe, M.A., Visser, R.J.W. & Stefels, J. (2014) The pigment composition of *Phaeocystis antarctica* (Haptophyceae) under various conditions of light, temperature, salinity, and iron. *Journal of Phycology*, 50, 1070–1080.

Lundholm, N., Hansen, P.J. & Kotaki, Y. (2004) Effect of pH on growth and domoic acid production by potentially toxic diatoms of the genera *Pseudo-nitzschia* and *Nitzschia*. *Marine Ecology Progress Series*, 273, 1–15.

Mackey, K.R.M., Paytan, A., Grossman, A.R. & Bailey, S. (2008) A photosynthetic strategy for coping in a high-light, low-nutrient environment. *Limnology and Oceanography*, 53, 900–913.

Maldonado, M.T., Hughes, M.P., Rue, E.L. & Wells, M.L. (2002) The effect of Fe and Cu on growth and domoic acid production by *Pseudo-*

*nitzschia multiserie*s and *Pseudo-nitzschia australis*. *Limnology and Oceanography*, 47, 515–526.

Maldonado, M.T., Allen, A.E., Chong, J.S., Lin, K., Leus, D., Karpenko, N. et al. (2006) Copper-dependent iron transport in coastal and oceanic diatoms. *Limnology and Oceanography*, 51, 1729–1743.

Marchetti, A., Maldonado, M.T., Lane, E.S. & Harrison, P.J. (2006) Iron requirements of the pennate diatom *Pseudo-nitzschia* Comparison of oceanic (high-nitrate, low-chlorophyll waters) and coastal species. *Limnology and Oceanography*, 51, 2092–2101.

Marchetti, A., Moreno, C.M., Cohen, N.R., Oleinikov, I., DeLong, K., Twining, B. et al. (2017) Development of a molecular-based index for assessing iron status in bloom-forming pennate diatoms. *Journal of Phycology*, 53, 820–832.

Martin, J.H., Gordon, R.M. & Fitzwater, S.E. (1990) Iron in Antarctic waters. *Nature*, 345, 156–158.

McMinn, A., Müller, M.N., Martin, A. & Ryan, K.G. (2014) The response of Antarctic sea ice algae to changes in pH and CO_2. *PLoS One*, 28, e86984. https://doi.org/10.1371/journal.pone.0086984

McQuaid, J.B., Kustka, A.B., Oborník, M., Horák, A., McCrow, J.P., Karas, B. et al. (2018) Carbonate-sensitive phytotransferrin controls high-affinity iron uptake in diatoms. *Nature*, 555, 534–537.

Mehrbach, C., Culberson, C., Hawley, J. & Pytkowicx, R. (1973) Measurements of the apparent dissociation constants of carbonic acid in seawater at atmospheric pressure. *Limnology and Oceanography*, 18, 897–907.

Mendes, C.R.B., Tavano, V.M., Leal, M.C., de Souza, M.S., Brotas, V. & Garcia, C.A.E. (2013) Shifts in the dominance between diatoms and cryptophytes during three late summers in the Bransfield Strait (Antarctic Peninsula). *Polar Biology*, 36, 537–547.

Mendes, C.R.B., Tavano, V.M., Dotto, T.S., Kerr, R., de Souza, M.S., CAE, G. et al. (2017) New insights on the dominance of cryptophytes in Antarctic coastal waters: a case study in Gerlache Strait. *Deep Sea Research Part II: Topical Studies in Oceanography*, 149, 161–170.

Moffat, C. & Meredith, M. (2018) Shelf-ocean exchange and hydrography west of the Antarctic Peninsula: A review. *Philosophical Transactions of the Royal Society A - Mathematical Physical and Engineering Sciences*, 376, 20170164.

Moline, M.A. & Prézelin, B.B. (1996) Long-term monitoring and analyses of physical factors regulating variability in coastal Antarctic phytoplankton biomass, in situ productivity and taxonomic composition over subseasonal, seasonal and interannual time scales. *Marine Ecology Progress Series*, 145, 143–160.

Moline, M.A., Claustre, H., Frazer, T.K., Schofield, O. & Vernet, M. (2004) Alteration of the food web along the Antarctic Peninsula in response to a regional warming trend. *Global Change Biology*, 10, 1973–1980.

Montes-Hugo, M., Doney, S., Ducklow, H., Fraser, W., Martinson, D., Stammerjohn, S. et al. (2009) Recent changes in phytoplankton communities associated with rapid regional climate change along the Western Antarctic Peninsula. *Science*, 323, 1470–1473.

Moreno, C.M., Lin, Y., Davies, S., Monbureau, E., Cassar, N. & Marchetti, A. (2018) Examination of gene repertoires and physiological responses to iron and light limitation in Southern Ocean diatoms. *Polar Biology*, 41, 679–696. https://doi.org/10.1007/s00300-017-2228-7

Olesen, A.J., Leithoff, A., Altenburger, A., Krock, B., Beszteri, B., Eggers, S. L. et al. (2021) First evidence of the toxin domoic acid in antarctic diatom species. *Toxins*, 13, 93. https://doi.org/10.3390/toxins13020093

Peers, G. & Price, N.M. (2006) Copper-containing plastocyanin used for electron transport by an oceanic diatom. *Nature*, 441, 341–344.

Petrou, K., Trimborn, S., Rost, B., Ralph, P.J. & Hassler, C.S. (2014) The impact of iron limitation on the physiology of the Antarctic diatom *Chaetoceros simplex*. *Marine Biology*, 161, 925–937.

Pierrot, D., Lewis, E., Wallace, D. (2006) MS excel program developed for CO_2 system calculations. ORNL/ CDIAC-105. U.S. Department of Energy

Prasil, O., Kolber, Z., Berry, J.A. & Falkowski, P.G. (1996) Cyclic electron flow around photosystem II in vivo. *Photosynthesis Research*, 48, 395–410.

Ralph, P.J. & Gademann, R. (2005) Rapid light curves: a powerful tool to assess photosynthetic activity. *Aquatic Botany*, 82, 222–237.

Raven, J.A., Evans, M.C.W. & Korb, R.E. (1999) The role of trace metals in photosynthetic electron transport in O_2-evolving organisms. *Photosynthesis Research*, 60, 111–149.

Redfield, A. (1958) The biological control of chemical factors in the environment. *American Scientist*, 46, 230A–221A.

Rue, E. & Bruland, K. (2001) Domoic acid binds iron and copper: a possible role for the toxin produced by the marine diatom *Pseudo-nitzschia*. *Marine Chemistry*, 76, 127–134.

Ryan-Keogh, T.J., Macey, A.I., Cockshutt, A.M., Moore, C.M. & Bibby, T.S. (2012) The cyanobacterial chlorophyll-binding-protein IsiA acts to increase the in vivo effective absorption cross-section of PSI under iron limitation. *Journal of Phycology*, 48, 145–154.

Schofield, O., Saba, G., Coleman, K., Carvalho, F., Couto, N. & Ducklow, H. (2017) Decadal variability in coastal phytoplankton community composition in a changing West Antarctic Peninsula. *Deep Sea Research Part I: Oceanographic Research Papers*, 124, 42–54. http://dx.doi.org/10.1016/j.dsr.2017.04.014

Semeniuk, D.M., Cullen, J.T., Johnson, W.K., Gagnon, K., Ruth, T.J. & Maldonado, M.T. (2009) Plankton copper requirements and uptake in the subarctic Northeast Pacific Ocean. *Deep-Sea Research Part I: Oceanography Research Papers*, 56, 1130–1142.

Smetacek, V., Klaas, C., Strass, V.H., Assmy, P., Montresor, M., Cisewski, B. et al. (2012) Deep carbon export from a Southern Ocean iron-fertilized diatom bloom. *Nature*, 487, 313–319.

Strzepek, R.F. & Harrison, P.J. (2004) Photosynthetic architecture differs in coastal and oceanic diatoms. *Nature*, 431, 689–692.

Strzepek, R.F., Maldonado, M.T., Hunter, K.A., Frew, R.D. & Boyd, P.W. (2011) Adaptive strategies by Southern Ocean phytoplankton to lessen iron limitation: uptake of organically complexed iron and reduced cellular iron requirements. *Limnology and Oceanography*, 56, 1983–2002.

Strzepek, R.F., Hunter, K.A., Frew, R.D., Harrison, P.J. & Boyd, P.W. (2012) Iron –light interactions differ in Southern Ocean phytoplankton. *Limnology and Oceanography*, 57, 1182–1200.

Suggett, D.J., MacIntyre, H.L. & Geider, R.J. (2004) Evaluation of biophysical and optical determinations of light absorption by photosystem II in phytoplankton. *Limnology and Oceanography*, 2, 316–332.

Suggett, D.J., Moore, C.M., Hickman, A.E. & Geider, R.J. (2009) Interpretation of fast repetition rate (FRR) fluorescence: Signatures of phytoplankton community structure versus physiological state. *Marine Ecology Progress Series*, 376, 1–19.

Sunda, W.G. & Huntsman, S.A. (1995) Iron uptake and growth limitation in oceanic and coastal phytoplankton. *Marine Chemistry*, 50, 189–206.

Thoisen, C., Riisgaard, K., Lundholm, N., Nielsen, T.G. & Hansen, P.J. (2015) Effect of acidification on an Arctic phytoplankton community from Disko Bay, West Greenland. *Marine Ecology Progress Series*, 520, 21–34.

Thomson, P.G., Davidson, A.T. & Maher, L. (2016) Increasing CO_2 changes community composition of pico- and nano-sized protists and prokaryotes at a coastal Antarctic site. *Marine Ecology Progress Series*, 554, 51–69.

Tortell, P.D., Payne, C.D., Li, Y., Trimborn, S., Rost, B., Smith, W.O. et al. (2008) CO_2 sensitivity of Southern Ocean phytoplankton. *Geophysical Research Letters*, 35, L04605.

Trimborn, S., Lundholm, N., Thoms, S., Richter, K., Krock, B., Hansen, P.J. et al. (2008) Inorganic carbon acquisition in potentially toxic and nontoxic diatoms: The effect of pH-induced changes in seawater carbonate chemistry. *Physiologia Plantarum*, 133, 92–105.

Trimborn, S., Brenneis, T., Sweet, E. & Rost, B. (2013) Sensitivity of Antarctic phytoplankton species to ocean acidification: growth, carbon acquisition, and species interaction. *Limnology and Oceanography*, 58, 997–1007.

Trimborn, S., Thoms, S., Brenneis, T., Heiden, J.P., Beszteri, S. & Bischof, K. (2017a) Two Southern Ocean diatoms are more sensitive to ocean acidification and changes in irradiance than the prymnesiophyte *Phaeocystis antarctica*. *Physiologia Plantarum*, 160, 155–170.

Trimborn, S., Brenneis, T., Hoppe, C.J.M., Laglera, L., Norman, L., Santos-Echeandía, J. et al. (2017b) Iron sources alter the response of Southern Ocean phytoplankton to ocean acidification. *Marine Ecology Progress Series*, 578, 35–50.

Trimborn, S., Thoms, S., Bischof, K. & Beszteri, S. (2019a) Susceptibility of two Southern Ocean phytoplankton key species to iron limitation and high light. *Frontiers in Marine Science*, 6, 1–17.

Trimborn, S., Thoms, S., Karitter, P. & Bischof, K. (2019b) Ocean acidification and high irradiance stimulate the photo-physiological fitness, growth and carbon production of the Antarctic cryptophyte *Geminigera cryophila*. *Biogeosciences*, 16, 2997–3008.

Wells, M.L., Trick, C.G., Cochlan, W.P., Hughes, M.P. & Trainer, V.L. (2005) Domoic acid: The synergy of iron, copper, and the toxicity of diatoms. *Limnology and Oceanography*, 50, 1908–1917.

Wu, S., Mi, T., Zhen, Y., Yu, K., Wang, F. & Yu, Z. (2021) A rise in ROS and EPS production: new insights into the *Trichodesmium erythraeum* response to ocean acidification. *Journal of Phycology*, 57, 172–182.

Young, J.N., Kranz, S.A., Goldman, J.A.L., Tortell, P.D. & Morel, F.M.M. (2015) Antarctic phytoplankton down-regulate their carbon-concentrating mechanisms under high CO_2 with no change in growth rates. *Marine Ecology Progress Series*, 532, 13–28.

Zhu, Z., Xu, K., Fu, F., Spackeen, J.L., Bronk, D.A. & Hutchins, D.A. (2016) A comparative study of iron and temperature interactive effects on diatoms and *Phaeocystis antarctica* from the Ross Sea, Antarctica. *Marine Ecology Progress Series*, 550, 39–51.

Zhu, Z., Qu, P., Gale, J., Fu, F. & Hutchins, D.A. (2017) Individual and interactive effects of warming and CO_2 on *Pseudo-nitzschia subcurvata* and *Phaeocystis antarctica*, two dominant phytoplankton from the Ross Sea, Antarctica. *Biogeosciences*, 14, 5281–5295.

SUPPORTING INFORMATION

Additional supporting information may be found in the online version of the article at the publisher's website.